



1 **The value of remote marine aerosol measurements for** 2 **constraining radiative forcing uncertainty**

3 Leighton A. Regayre¹, Julia Schmale², Jill S. Johnson¹, Christian Tatzelt³, Andrea Baccharini²,
4 Silvia Henning³, Masaru Yoshioka¹, Frank Stratmann³, Martin Gysel-Beer² and Ken S.
5 Carslaw¹

6
7 ¹Institute for Climate and Atmospheric Science, School of Earth and Environment, University of Leeds, Leeds,
8 LS2 9JT, UK

9 ²Paul Scherrer Institute, Laboratory of Atmospheric Chemistry, Villigen, Switzerland

10 ³Leibniz Institute for Tropospheric Research, Leipzig, Germany

11

12 *Correspondence to:* Leighton Regayre (L.A.Regayre@leeds.ac.uk)

13 *Correspondence related to measurements to:* Julia Schmale (julia.schmale@psi.ch)

14

15 **Abstract.** Aerosol measurements over the Southern Ocean are used to constrain aerosol-
16 cloud interaction radiative forcing uncertainty in a global climate model. Aerosol forcing
17 uncertainty is quantified using one million climate model variants that sample the uncertainty
18 in nearly 30 model parameters. Ship-based measurements of cloud condensation nuclei,
19 particle number concentrations and sulfate mass concentrations from the Antarctic
20 Circumnavigation Expedition: Study of Preindustrial-like Aerosols and Their Climate Effects
21 (ACE-SPACE) are used to identify observationally implausible variants and thereby reduce
22 the spread in the simulated forcing. Southern Ocean measurements strongly constrain natural
23 aerosol emissions: default sea spray emissions in the model need to be increased by around a
24 factor of 3 to be consistent with measurements. Aerosol forcing uncertainty is reduced by
25 around 7% using these measurements, which is comparable to the 8% reduction achieved
26 using an extensive set of over 9000 predominantly Northern Hemisphere measurements. The
27 radiative forcing due to aerosol-cloud interactions (RF_{aci}) is constrained to -2.61 to -1.10 W
28 m^{-2} (95% confidence) and the effective radiative forcing from aerosol-cloud interactions
29 (ERF_{aci}) is constrained to -2.43 to -0.54 W m^{-2} . When Southern Ocean and Northern
30 Hemisphere measurements are combined, the uncertainty in RF_{aci} is reduced by 21% and the
31 strongest 20% of forcing values are ruled out as implausible. In this combined constraint the
32 observationally plausible RF_{aci} is around 0.17 W m^{-2} weaker (less negative) with credible
33 values ranging from -2.51 to -1.17 W m^{-2} and from -2.18 to -1.46 W m^{-2} when using one
34 standard deviation to quantify the uncertainty. The Southern Ocean and Northern Hemisphere
35 measurement datasets are complementary because they constrain different processes. These
36 results highlight the value of remote marine aerosol measurements.

37

38

39 **1 Introduction**

40 The uncertainty in the magnitude of the effective radiative forcing caused by aerosol-cloud interactions (ERF_{aci})
41 due to changing emissions over the industrial period is around twice that for CO_2 (Stocker et al., 2013). It is
42 essential to reduce this uncertainty if global climate models are to be used to robustly predict near-term changes
43 in climate (Andreae et al., 2005, Myhre et al., 2013, Collins et al., 2013, Tett et al., 2013, Seinfeld et al., 2016).
44

45 Aerosol forcing uncertainty has persisted in climate models since the 1990s partly because there are no
46 measurements covering the industrial period that can be used to directly constrain simulations of long-term
47 changes in aerosol and cloud properties (Grypsperdt et al., 2017; McCoy et al., 2017). Estimates of aerosol



48 forcing over the industrial period therefore rely on models that have been evaluated against measurements made
49 in the present-day atmosphere. However, it is known that the aerosol forcing (in particular the component
50 caused by aerosol-cloud interactions) depends sensitively on the state of aerosols in the pre-industrial period
51 (Carslaw et al., 2013; Wilcox et al. 2015) when natural aerosols were dominant (Carslaw et al., 2017).
52 Observations of natural aerosols in the present-day atmosphere are therefore expected to help constrain the
53 simulated forcing unless there have been significant changes in natural aerosol processes over the industrial
54 period, for which there is little evidence (Carslaw et al., 2010).

55
56 In this paper we address the questions: i) To what extent can measurements of aerosols in pristine (natural)
57 environments help to constrain model simulations and thereby reduce the large uncertainty in aerosol forcing?
58 ii) What is the relative importance of measurements in remote and polluted environments for constraining the
59 forcing uncertainty? It is known that the abundance of natural aerosols affects the magnitude of forcing in a
60 model (Spracklen and Rap, 2013; Carslaw et al., 2013). However, to assess the effect on the *uncertainty* in
61 forcing it is necessary to explore how the spread of predictions of a set of models changes when constrained by
62 measurements. The 5th Coupled Model Intercomparison Project is inadequate for this purpose because of
63 insufficient aerosol diagnostics (Wilcox et al., 2015). Here we use large perturbed parameter ensembles (PPEs)
64 of the UK Hadley Centre General Environment Model HadGEM3 (Hewitt et al, 2011). The PPEs were created
65 by systematically perturbing numerous model parameters related to natural and anthropogenic emissions and
66 physical processes. The simulated aerosol forcings have uncertainty ranges that exceed those of multi-model
67 ensembles (Yoshioka et al., 2019; Johnson et al., 2019). Instantaneous radiative forcing (RF) is quantified using
68 the 26-parameter AER PPE in which just aerosol-related parameters were varied, and the effective radiative
69 forcing (ERF) is quantified using the 27-parameter AER-ATM PPE in which aerosol and physical atmosphere
70 parameters were varied (Yoshioka et al., 2019). We use these PPEs to quantify how the constraint provided by
71 pristine aerosol measurements affects the spread of aerosol forcings simulated by the ensembles.

72
73 Previous analysis of HadGEM3 PPEs showed that measurements of the present-day atmosphere in regions
74 affected by anthropogenic emissions have limited impact on the uncertainty in simulated aerosol forcing. For
75 example, Regayre et al., (2018) showed that top-of-the-atmosphere shortwave radiation flux measurements
76 reduce ERF_{aci} uncertainty by only around 10%, despite the fluxes in the present-day and early-industrial
77 environments sharing multiple causes of uncertainty. Johnson et al. (2019) showed that a much larger dataset of
78 over 9000 (predominantly Northern Hemisphere) aerosol measurements constrained the global, annual mean
79 aerosol RF uncertainty by only around 8%. These measurements reduce the uncertainty in a small number of
80 parameters related to anthropogenic emissions and aerosol processing in polluted environments. However,
81 important causes of uncertainty in RF_{aci} , such as natural aerosol emission fluxes, were largely unconstrained.

82
83 The Southern Ocean is one of the few regions on Earth (along with some boreal forests) in which the same
84 processes are expected to affect cloud-active aerosol concentrations in the present-day and early-industrial
85 atmospheres (Hamilton et al., 2014). In this study we make use of aerosol measurements from the Antarctic
86 Circumnavigation Expedition: Study of Preindustrial-like Aerosols and Their Climate Effects (ACE-SPACE)
87 campaign (Schmale et al., 2019). They offer a unique opportunity to constrain the early-industrial aspects of
88 aerosol forcing uncertainty because the Southern Ocean is a source of natural aerosols that are relevant at the
89 global scale and remains largely unaffected by anthropogenic aerosol and precursor emissions.

90
91 We use near-surface measurements of cloud condensation nuclei concentrations at 0.2% and 1.0%
92 supersaturations ($CCN_{0.2}$ and $CCN_{1.0}$; Tatzelt et al., 2019), as well as mass concentrations of non-sea-salt sulfate
93 in PM_{10} and number concentrations of particles larger than 700 nm (N_{700} ; Schmale et al., 2019a). The
94 measurements are compared to output from 1 million variants of the HadGEM3 model that sample combinations
95 of parameter settings in the model. These model variants are used to represent aerosol forcing uncertainty in our
96 model using probability density functions (pdfs) and were generated by sampling from Gaussian Process
97 emulators that were trained on the PPE model outputs (see SI Methods). Model variants that were judged to be
98 observationally implausible against the measurements were rejected, resulting in a set of plausible variants from
99 which the uncertainty in aerosol forcing could be computed (see SI Methods). In the results shown below, we
100 retained approximately 3% of model variants (following Johnson et al., 2019) that best match all four measured
101 aerosol properties.

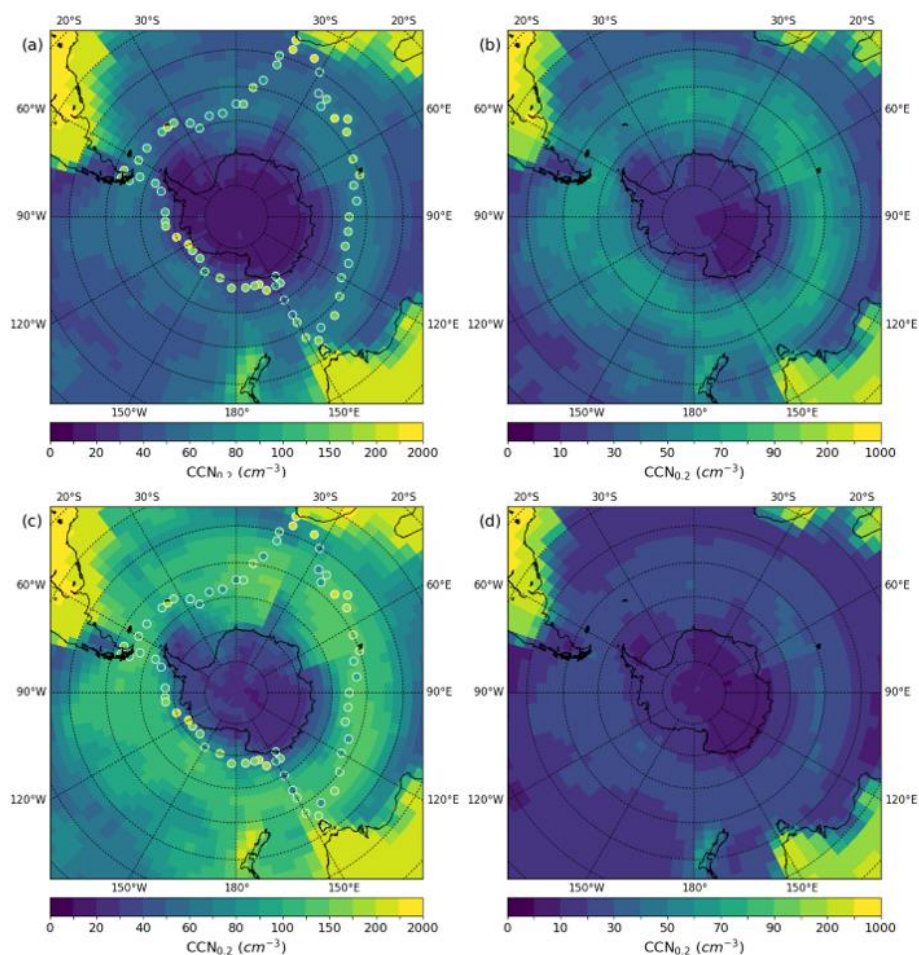
102
103



104 **2 Results**

105

106 Fig. 1 shows the $CCN_{0.2}$ mean and standard deviation from the unconstrained and constrained model variants to
107 exemplify the effect of constraint on model output. The mean concentrations in the unconstrained sample are
108 much smaller than measured concentrations. However, the range of $CCN_{0.2}$ values in the unconstrained sample
109 spans the measurements in most locations (Fig. 1b). The measurement constraint increases $CCN_{0.2}$
110 concentrations (more than double the unconstrained mean in many locations; Fig. 1c) and greatly reduces the
111 $CCN_{0.2}$ uncertainty (by more than half everywhere to less than 50 cm^{-3} ; Fig. 1d).
112



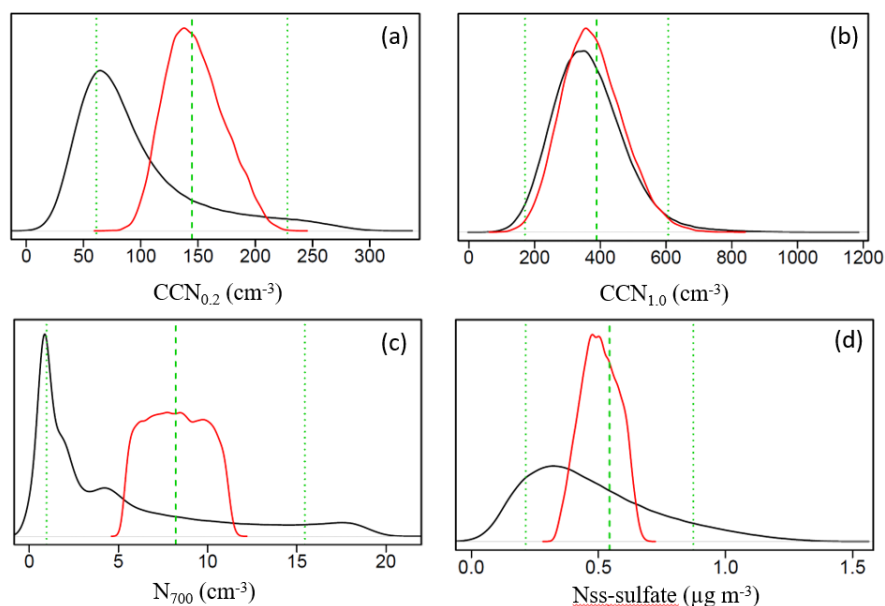
113

114 Fig. 1. a,c) Mean and b,d) standard deviation of $CCN_{0.2}$ concentrations from the a,b) unconstrained sample and c,d) the
115 sample constrained using concentration measurements of $CCN_{0.2}$, $CCN_{1.0}$, non-sea-salt sulfate and particle numbers larger
116 than 700 nm. Measured $CCN_{0.2}$ values are plotted as dots. Means and standard deviations were calculated using samples
117 taken from emulators trained using monthly mean values. December to March sample values were combined based on
118 longitudinal agreement with measurements.
119

120 Fig. 2 shows pdfs of the output from the model for the four variables used as constraints, calculated as means
121 over the locations where measurements were taken. The constraint reduces the uncertainty in all measurement
122 types (narrower pdfs) and the central tendency of the pdfs is closer to the regional mean of measurements after



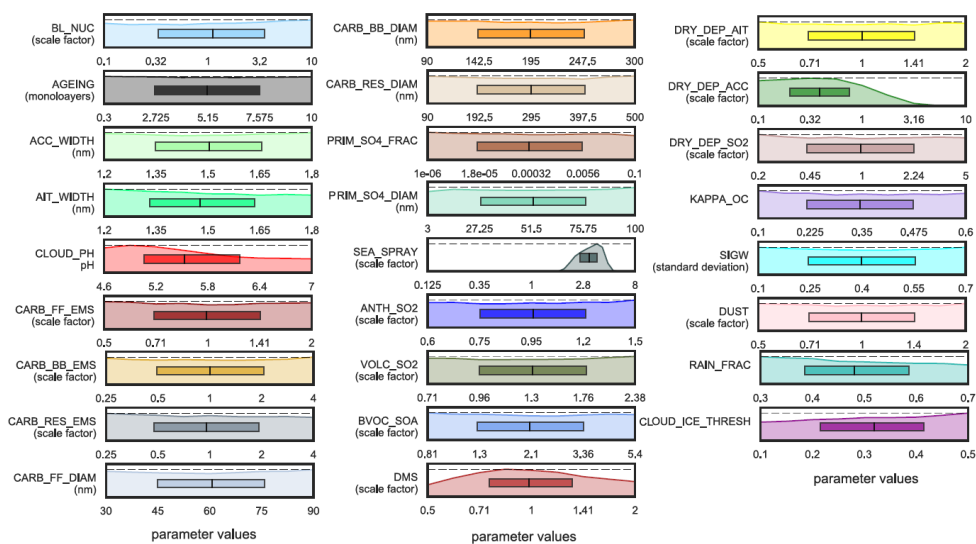
123 constraint. Rejecting around 97% of model variants as implausible compared to measurements greatly improves
124 the model-measurement comparison.
125



126
127
128
129
130
131
132
133
134
135
136
137
138
139
140

Fig. 2. Unconstrained (black) and observationally constrained (red) pdfs of aerosol properties: a) $CCN_{0.2\%}$, b) $CCN_{1.0\%}$, c) N_{700} and d) aerosol sulfate. The pdfs were calculated at locations where measurements were used for constraint across the months December to March. The green dashed line shows the median of the measurements and the dotted green lines show the approximate uncertainty ranges that were accounted for in the constraint (See SI Methods).

After constraint, the remaining model variants inhabit specific parts of the 26-dimensional parameter uncertainty space used to quantify the model uncertainty. We explore the effect of constraints on parameter values using 1-dimensional marginal probability distributions (described in detail in Johnson et al., 2019) – see Fig. 3 and Fig. S1 for equivalent AER-ATM results. The magnitude of the marginal probability distribution after constraint reflects the number of ways in which a particular value of a parameter can be combined with settings of all the other parameters to produce an observationally plausible model. The white space in the marginal pdfs shows where parameter value density has decreased.



141
 142
 143
 144
 145
 146
 147
 148
 149
 150
 151
 152
 153
 154
 155
 156
 157
 158
 159
 160
 161
 162
 163
 164
 165
 166
 167
 168
 169
 170
 171
 172
 173
 174
 175
 176
 177
 178
 179
 180

Fig. 3. Marginal probability distributions for the 26 aerosol parameters after constraint using ACE-SPACE measurements. The density of parameter values in the unconstrained sample are shown as dashed lines. Densities of constrained samples are shown in colour and are scaled so that the maximum densities in the constrained and unconstrained samples are aligned. The 25th, 50th and 75th percentiles of each marginal distribution are shown in the central boxes. Parameter values on the x-axes correspond to values used in the model (Yoshioka et al., 2019).

The relative simplicity of aerosol emissions and processes over the Southern Ocean (compared to polluted continental regions) means that measurements can be used to tightly constrain uncertainty in the associated parameters. Two parameters, sea spray emissions and dry deposition velocity, are tightly constrained such that some parameter values are ruled out as implausible. Several other parameters (related to cloud droplet pH, DMS emissions and wet deposition) are more modestly constrained. These constraints suggest the model-measurement comparison is improved when aerosol number concentrations and mass are relatively high.

Sea spray emissions are tightly constrained to be around 3 times larger than the default model value. Observationally plausible values of the sea spray scaling parameter range from around 1.6 to 5.1 and all other values (including the default emission calculated in the model) are ruled out as implausible. This suggests that sea spray emissions in our model need to be significantly higher than those calculated using the wind speed dependent Gong (2003) parametrisation. We do not make any assumptions about the composition of these additional sea spray particles. They may be rich in organic material as proposed by Gantt et al., (2011) which would alter the CCN activity of emitted particles. However, the consistency of constraint of CCN0.2 and N700 towards higher values (Fig. 1) implies that a general scaling of the existing sea spray flux is consistent with the measurements without the need for an additional source of fine-mode, organic-rich particles.

These results conflict with the findings of Revell et al. (2019) who suggest the relatively simple wind speed dependent nature of the Gong (2003) parametrisation produces too much sea spray aerosol over the Southern Ocean from December to February. If Revell et al. (2019) had sampled a wider range of processes (such as deposition) as we have here, our results might be brought into agreement. A better understanding of these conflicting results could be achieved using a multi-model experiment that sampled a range of atmospheric process representations.

The dry deposition velocity of accumulation mode aerosols (Dry_Dep_Acc) has an 84% likelihood of being lower than the default model value after applying the constraint. Furthermore, deposition velocities larger than around 3 times the default value are effectively ruled out. This constraint is consistent with the higher aerosol concentrations implied by constraint of the sea spray emission parameter.

Other parameters are more modestly constrained. The constraint on the scaled DMS emission flux is two-sided, reducing the credible range of DMS emission scalings from 0.5 to 2.0 down to 0.54 to 1.9. This constraint suggests the default emission inventory is consistent with measurements and doesn't benefit from being scaled.



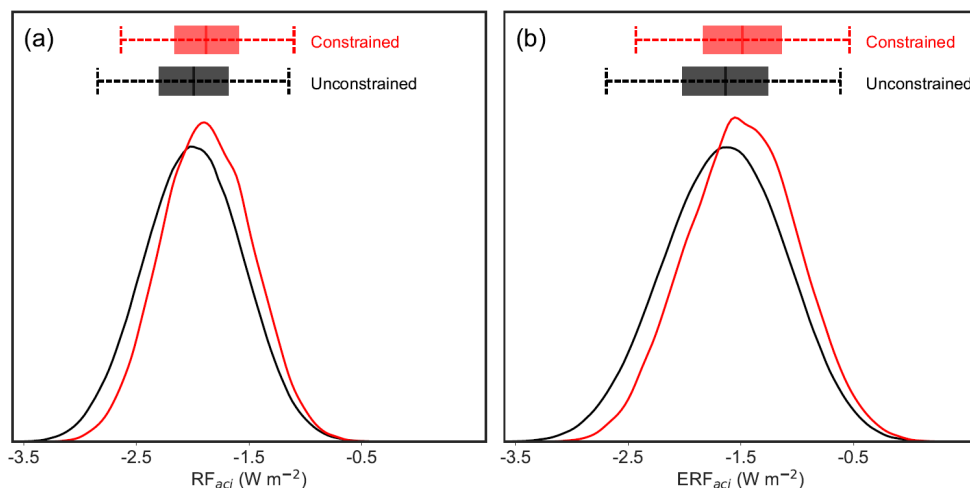
181 Furthermore, ACE-SPACE measurements are consistent with less efficient aerosol scavenging (55% likelihood
182 of Rain_Frac, the parameter that controls the proportion of cloudy model grid boxes where rain occurs, being
183 below 0.5) and less aqueous phase sulfate production (pH of cloud droplets has a 62% likelihood of being lower
184 than the unconstrained median value). These combined constraints suggest, in agreement with sea spray and
185 deposition parameter constraints, higher aerosol number and mass concentrations are consistent with
186 measurements.

187

188 The effects of measurement constraint on pdfs of RF_{aci} and ERF_{aci} are shown in Fig. 4. Removing implausible
189 model variants has reduced the uncertainty in several parameters including natural aerosol emission fluxes,
190 which translates into a reduction in RF_{aci} uncertainty (Carslaw et al., 2013). The measurement constraints have
191 two important effects on aerosol forcing. Firstly, the magnitude of median RF_{aci} weakens from -1.99 W m^{-2} to
192 -1.88 W m^{-2} (-1.64 to -1.49 W m^{-2} for ERF_{aci}). A weaker forcing is consistent with higher natural aerosol
193 emissions and increased aerosol load in the early-industrial period. Secondly, the constrained forcing pdfs are
194 approximately symmetric but have shorter tails (lower kurtosis). This suggests the constraints are selectively
195 ruling out model variants that are outliers. The 95% credible range of RF_{aci} values is reduced by around 9%
196 (from -2.84 to -1.15 W m^{-2} down to -2.64 to -1.10 W m^{-2}) and around 9% for ERF_{aci} (from -2.69 to -0.62 W m^{-2}
197 down to -2.43 to -0.54 W m^{-2}). The consistency of forcing constraint across two distinct PPEs suggests the
198 results are insensitive to differences in meteorology, parameters perturbed in the PPEs, and the inclusion of
199 rapid atmospheric adjustments. These results are also insensitive to additional constraint to ensure energy
200 balance at the top of the atmosphere (Fig. S2).

201

202



203

204

205 Fig. 4. Probability distributions of a) RF_{aci} and b) ERF_{aci} . The distributions of the unconstrained sample of one million model
206 variants from statistical emulators of each PPE are in black. Red lines show the distributions after constraint using ACE-
207 SPACE measurements (around 3% of the unconstrained sample). The 25th, 50th and 75th percentiles of each sample are
208 shown as shaded boxes and dashed lines span the 2.5th and 97.5th percentiles.

209

210

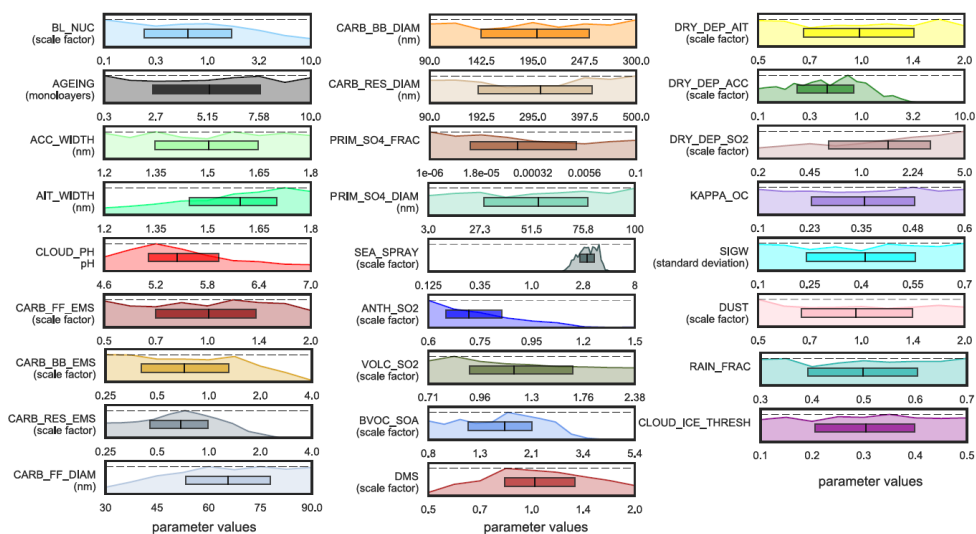
211 Johnson et al. (2019) reduced the global, annual mean RF_{aci} uncertainty by constraining multiple anthropogenic
212 emission and model process parameters (as well as some natural aerosol parameters) using over 9000
213 predominantly Northern Hemisphere measurements of aerosol optical depth, $PM_{2.5}$, particle number
214 concentrations and mass concentrations of organic carbon and sulfate. We used the same methodology as
215 Johnson et al. (2019) to rule out implausible model variants from the same original sample of one million model
216 variants, so we can readily combine these constraints. Around 700 model variants (0.07%) are observationally
217 plausible in both the Southern Ocean (ACE-SPACE) and Johnson et al. (2019) constraints. The marginal
218 parameter pdfs from this 700-member sample are shown in Fig. 5. Because Johnson et al. studied only the AER
219 PPE (from which RF_{aci} can be computed) we are unable to explore the effect of the combined constraint on
220 ERF_{aci} .

221

222



223



224

225

226

227

228

229

230

231

232

233

234

235

236

237

238

239

240

241

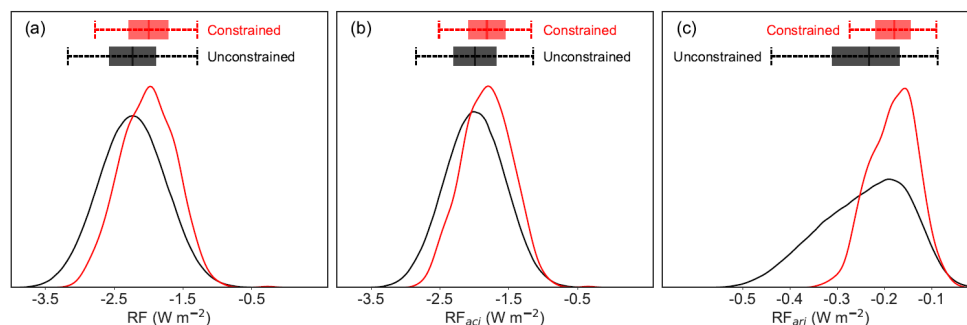
242

243

Fig. 5. Marginal probability distributions for the 26 aerosol parameters after constraint using around 250 Southern Ocean measurements and more than 9000 aerosol measurements in Johnson et al. (2019). Plotting features of this figure are identical to Fig. 3.

The two measurement datasets constrain distinct groups of parameters. There are a few cases where the same parameters are constrained by both datasets and in these cases the parameter values are constrained consistently (e.g. cloud droplet pH) or more strongly through ACE-SPACE (e.g. sea spray emissions). The complementary nature of these constraints means that the combined constraint marginal parameter pdfs (Fig. 5) are remarkably similar to those in our Fig. 3e (for sea spray and DMS emission fluxes, as well as deposition and pH parameters) and in figure 6 of Johnson et al. (2019) for other parameters.

The Johnson et al. (2019) constraint reduced the RF_{aci} uncertainty by around 6% and our ACE-SPACE measurement constraint reduced the uncertainty by around 9%. However, the RF_{aci} uncertainty is reduced by around 21% (Fig. 6a) after applying both constraints, meaning the combined constraint is stronger than the sum of individual constraints.



244

245

246

247

248

249

250

Fig. 6. Probability distributions of a) RF , b) RF_{aci} and c) RF_{ari} from the unconstrained (black line) and constrained (red line) samples of model variants. The constrained sample includes model variants that agree with our ACE-SPACE measurement constraint and the Johnson et al. (2019) constraint. Plotting features are identical to Fig. 4.

The Johnson et al. (2019) constraint strengthened the RF_{aci} by around 0.3 W m^{-2} because the largest sea spray emission flux scaling and largest new particle formation rates were ruled out. Our ACE-SPACE constraint rules



251 out the same large sea spray emission fluxes, but also rules out all emission flux scale factors lower than around
252 1.6, which increases the baseline aerosol concentration in the early-industrial atmosphere. The ACE-SPACE
253 measurements also constrain several other parameters that collectively weaken RF_{aci} weaken the median RF_{aci} by
254 around 0.18 W m^{-2} . Therefore, using the combined measurement dataset, the highest and lowest RF_{aci} values
255 have been ruled out as implausible and the credible range of observationally plausible RF_{aci} values is reduced to
256 around -2.51 to -1.17 W m^{-2} (-2.18 to -1.46 W m^{-2} , when using one standard deviation to quantify the
257 uncertainty). Uncertainty in RF_{ari} is reduced by around 48% with observationally plausible values ranging from -
258 0.27 to -0.09 W m^{-2} (-0.23 to -0.13 W m^{-2} , when using one standard deviation), because the strongest RF_{ari}
259 values are ruled out as observationally implausible.
260

261 3 Discussion

262
263 Our results show, as hypothesised from previous sensitivity analyses, that remote marine measurements are
264 valuable for constraining the natural aerosol state of the atmosphere (Carslaw et al., 2013; Regayre et al., 2014;
265 Regayre et al., 2018). Remote marine aerosol measurements provide new information about plausible model
266 behaviour because they are closely related to model emissions and processes that measurements in polluted
267 environments do not constrain.
268

269 For the first time we have achieved a meaningful reduction of 21% in the RF_{aci} uncertainty by constraining the
270 aerosol properties in the model. The reduction in forcing uncertainty can still be improved by considering the
271 following: Firstly, there are several causes of RF_{aci} uncertainty that are not constrained by a combination of
272 Northern Hemisphere and pristine Southern Ocean measurements. Identifying measurements associated with
273 primary particle emission diameters (BB_{diam} and $Prim_{SO4_{diam}}$), Aitken mode aerosol removal rates
274 ($Dry_{Dep_{Ait}}$) and model process parameters related to cloud droplet activation ($Kappa_{OC}$, Ait_{width} ,
275 Sig_W) and using them as additional constraints should further reduce the forcing uncertainty. Secondly, even
276 within the considerably reduced volume of multi-dimensional parameter space there still exist many
277 compensating parameter effects, which limit the constraint on individual parameter ranges (Lee et al., 2016;
278 Regayre et al., 2018). The impact of these compensating effects could be greatly reduced by perturbing
279 uncertain emissions regionally rather than globally as we do here.
280

281 Our results are based on uncertainty in a single climate model. Model inter-comparison projects (such as
282 CMIP6) can be used to quantify the diversity of RF (or ERF) output from models, but they lack information
283 about single model uncertainty. Ideally, multi-model ensembles would contain a perturbed parameter
284 component, but the computational cost prevents many modelling groups from engaging with this important
285 aspect of uncertainty quantification, limiting our shared knowledge about the causes of aerosol forcing
286 uncertainty. Studies like ours that quantify the remaining uncertainty in aerosol forcing and its components after
287 constraint using multiple measurement types fill an important knowledge gap. This knowledge can be used to
288 form a more complete understanding of the importance of historical and near-term aerosol radiative forcing
289 which would reduce the diversity in equilibrium climate sensitivity across models.
290
291

292 Data availability

293 The ACE-SPACE data are accessible from: <https://zenodo.org/communities/spi-ace>. Simulation output data in
294 both AER and AER-ATM PPEs are available on the JASMIN data infrastructure (<http://www.jasmin.ac.uk>).
295 Some of the climate-relevant fields are derived and stored in netCDF files (.nc) containing data for all ensemble
296 members and made available as a community research tool as described in Yoshioka et al. (2019). Model data
297 and analysis code can be made available from the corresponding author upon request.



298 Author Contribution

299 LR applied the statistical methodology and generated results. LR and MY created the PPEs. LR and JJ designed
300 the experiments and elicited probability density functions of all aerosol parameters. KC and MY participated in
301 the formal elicitation process. JS, AB, MG, CT, SH and FS collected and processed the ACE-SPACE
302 measurements. LR, KS, JS and JJ analysed the results. LR and KS wrote the manuscript with contributions from
303 all authors.

304 Competing Interests

305 Author KC is an executive editor of ACP.

306 Acknowledgements

307 We acknowledge funding from NERC under grants AEROS, ACID-PRUF, GASSP and A-CURE
308 (NE/G006172/1, NE/I020059/1, NE/J024252/1 and NE/P013406/1) and the European Union ACTRIS-2 project
309 under grant 262254. This work and its contributors (LR, JJ and KC) were supported by the UK-China Research
310 & Innovation Partnership Fund through the Met Office Climate Science for Service Partnership (CSSP) China
311 as part of the Newton Fund. MY and KS received funding from the National Centre for Atmospheric Science
312 (NCAS), one of the UK Natural Environment Research Council (NERC) research centres via the ACSIS long-
313 term science programme on the Atlantic climate system. LR was funded by a Natural Environment Research
314 Council (NERC) Doctoral Training Grant, and a CASE studentship with the UK Met Office Hadley Centre. KC
315 is currently a Royal Society Wolfson Merit Award holder. ACE-SPACE, JS, SH and AB received funding from
316 EPFL, the Swiss Polar Institute and Ferring Pharmaceuticals. ACE-SPACE was carried out with additional
317 support from the European FP7 project BACCHUS (grant agreement no. 49603445). AB received funding from
318 the Swiss National Science Foundation grant No. 200021_169090. This work used the ARCHER UK National
319 Supercomputing Service (<http://www.archer.ac.uk>). ARCHER project allocations n02-chem, n02-NEJ024252,
320 n02-FREEPPE and the Leadership Project allocation n02-CCPPE were used to perform sensitivity tests and
321 create the ensembles. We thank Andre Welti and Markus Hartmann for CCN measurement support provided
322 during the ACE-SPACE campaign.

323

324 References

- 325 Andreae, M. O., Jones, C. D., and Cox, P. M.: Strong present-day aerosol cooling implies a hot future, *Nat.*, 435,
326 1187–1190, doi:10.1038/nature03671, 2005.
327
328 Carslaw, K. S., Boucher, O., Spracklen, D. V., Mann, G. W., Rae, J. G. L., Woodward, S., and Kulmala, M.: A
329 review of natural aerosol interactions and feedbacks within the Earth system, *Atmos. Chem. Phys.*, 10,
330 1701–1737, 10.5194/acp-10-1701-2010, 2010.
331
332 Carslaw, K. S., Lee, L. A., Reddington, C. L., Pringle, K. J., Rap, A., Forster, P. M., Mann, G.W., Spracklen, D.
333 V., Woodhouse, M., Regayre, L. A., and Pierce, J. R.: Large contribution of natural aerosols to uncertainty
334 in indirect forcing, *Nat.*, 503, 67–71, doi:10.1038/nature12674, 2013.
335
336 Carslaw, K. S., Gordon, H., Hamilton, D. S., Johnson, J. S., Regayre, L. A., and Yoshioka, M.: Aerosols in the
337 pre-industrial atmosphere, *Curr. Clim. Change Rep.*, 3, 1–15, doi:10.101007/s40641-017-0061-2, 2017.
338
339 Collins, M., Knutti, R., Arblaster, J., Dufresne, J. L., Fichet, D., Friedlingstein, P., Gao, X., Gutowski, W. J.,
340 Johns, T., Krinner, G., Shongwe, M., Tebaldi, C., Weaver, A. J., and Wehner, M.: Long-term Climate
341 Change: Projections Commitments and Irreversibility, in: *Climate Change 2013: The Physical Science*
342 *Basis. Contribution of Working Group I to the Fifth Assessment Report of the Intergovernmental Panel on*



- 343 Climate Change, edited by Stocker, T. F., Qin, D., Plattner, G. K., Tignor, M., Allen, S. K., Boschung, J.,
344 Nauels, A., Xia, Y., Bex, V., and Midgley, P. M., Cambridge University Press, Cambridge, United Kingdom
345 and New York, NY, USA, 2013.
- 346
- 347 Gantt, B., Meskhidze, N., Facchini, M.C., Rinali, M., Ceburnis, D. and O'Dowd, C.D.: Wind speed dependent
348 size-resolved parameterization for the organic mass fraction of sea spray aerosol, *Atmos. Chem. Phys.*,
349 11, 8777–8790, doi:10.5194/acp-11-8777-2011, 2011.
- 350
- 351 Gong, S. L.: A parameterization of sea-salt aerosol source function for sub- and super-micron particles, *Glob.*
352 *Biogeochem. Cyc.*, 17, 1097, doi:10.1029/2003GB002079, 2003.
- 353
- 354 Gryspeerd, E., Quaas, J., Ferrachat, S., Gettelman, A., Ghan, S., Lohmann, U., Morrison, H., Neubauer, D.,
355 Partridge, D. G., Stier, P., Takemura, T., Wang, H., Wang, M., and Zhang, K.: Constraining the
356 instantaneous aerosol influence on cloud albedo, *Proc. Natl. Acad. Sci.*, 114, 4899–4904,
357 doi:10.1073/pnas.1617765114, 2017.
- 358
- 359 Hamilton, D. S., Lee, L. A., Pringle, K. J., Reddington, C. L. S., Spracklen, D. V., and Carslaw, K. S.: Occurrence
360 of pristine aerosol on a polluted planet, *Proc. Natl. Acad. Sci.*, 111, 18 466–18 471,
361 doi:10.1073/pnas.1415440111, 2014.
- 362
- 363 Hewitt, H. T., Copey, D., Culverwell, I. D., Harris, C. M., Hill, R. S. R., Keen, A. B., McLaren, A. J., and Hunke,
364 E. C.: Design and implementation of the infrastructure of HadGEM3: the next-generation Met Office
365 climate modelling system, *Geosci. Mod. Dev.*, 4, 223–253, doi:10.5194/gmd-4-223-2011, 2011.
- 366
- 367 Johnson, J. S., Regayre, L. A., Yoshioka, M., Pringle, K. J., Turnock, S. T., Browse, J., and Carslaw, K. S.:
368 Robust observational constraint of processes and emissions in a climate model and the effect on aerosol
369 radiative forcing, *Atmos. Chem. Phys. Discuss.*, doi:10.5194/acp-2019-834, in review, 2019.
- 370
- 371 Lee, L. A., Reddington, C. L., and Carslaw, K. S.: On the relationship between aerosol model uncertainty and
372 radiative forcing uncertainty, *Proc. Natl. Acad. Sci.*, 113, 5820–5827, doi:10.1073/pnas.1507050113,
373 2016.
- 374
- 375 McCoy, D. T., Bender, F. A., Mohrmann, J. K. C., Hartmann, D. L., Wood, R., and Grosvenor, D. P.: The global
376 aerosol-cloud first indirect effect estimated using MODIS, MERRA, and AeroCom, *JGRA*, 122, 1779–
377 1796, doi:10.1002/2016JD026141, 2017.
- 378
- 379 Myhre, G., Shindell, D., Bréon, F. M., Collins, W., Fuglested, J., Huang, J., Koch, D., Lamarque, J. F., Lee, D.,
380 Mendoza, B., Nakajima, T., Robock, A., Stephens, G., Takemura, T., and Zhang, H.: Anthropogenic and
381 Natural Radiative Forcing, in: *Climate Change 2013: The Physical Science Basis. Contribution of Working
382 Group I to the Fifth Assessment Report of the Intergovernmental Panel on Climate Change*, edited by
383 Stocker, T. F., Qin, D., Plattner, G. K., Tignor, M., Allen, S. K., Boschung, J., Nauels, A., Xia, Y., Bex, V.,
384 and Midgley, P. M., Cambridge University Press, Cambridge, United Kingdom and New York, NY, USA,
385 2013.
- 386
- 387 Regayre, L. A., Pringle, K. J., Booth, B. B. B., Lee, L. A., Mann, G. W., Browse, J., Woodhouse, M. T., Rap, A.,
388 Reddington, C. L. S., and Carslaw, K. S.: Uncertainty in the magnitude of aerosol-cloud radiative forcing
389 over recent decades, *Geophys. Res. Lett.*, 41, 9040–9049, doi:10.1002/2014GL062029, 2014.
- 390
- 391 Regayre, L. A., Johnson, J. S., Yoshioka, M., Pringle, K. J., H.Sexton, D. M., Booth, B. B. B., Lee, L. A., Bellouin,
392 N., and Carslaw, K. S.: Aerosols and physical atmosphere model parameters are both important sources
393 of uncertainty in aerosol ERF, *ACP*, 18, 9975–10 006, doi:10.5194/acp-18-9975-2018, 2018.
- 394
- 395 Revell, L. E., Kremser, S., M. Harvey, S. H., Mulcahy, J. P., Williams, J., Morgenstern, O., McDonald, A. J.,
396 Varma, V., Bird, L., and Schuddeboom, A.: The sensitivity of Southern Ocean aerosols and cloud
397 microphysics to sea spray and sulfate aerosol production in the HadGEM3-GA7.1 chemistry-climate
398 model, *Atmos. Chem. Phys. Discuss.*, 19, doi:10.5194/acp-2019-629, 2019.
- 399
- 400 Schmale, J., Baccharini, A., Thurnherr, I., Henning, S., Efraim, A., Regayre, L. A., Bolas, C., Hartmann, M., Welti,
401 A., Lehtipalo, K., Aemisegger, F., Tatzelt, C., Landwehr, S., Modini, R., Tummon, F., Johnson, J. S.,
402 Harris, N., Schnaiter, M., Toffoli, A., Derkani, M., Bukowiecki, N., Stratmann, F., Dommen, J.,
403 Baltensperger, U., Wernli, H., Rosenfeld, D., Gysel-Beer, M., and Carslaw, K.: Overview of the Antarctic
404 Circumnavigation Expedition: Study of Preindustrial-like Aerosols and Their Climate Effects (ACE-
405 SPACE), *Bull. Amer. Meteorol. Soc.*, Early Online Release, doi:10.1175/BAMS-D-18-0187.1, 2019.
- 406
- 407 Schmale, J., Henning, S., Tummon, F., Hartmann, M., Baccharini, A., Welti, A., Lehtipalo, K., Tatzelt, C.,
408 Landwehr, S. and Gysel-Beer, M.: Course mode aerosol particle size distribution collected in the Southern



- 409 Ocean in the austral summer of 2016/2017, during the Antarctic Circumnavigation Expedition, Version 1.0
410 Dataset, doi:10.5281/zenodo.2636709, 2019a.
411
- 412 Seinfeld, J. H., Bretherton, C., Carslaw, K. S., Coe, H., DeMott, P. J., Dunlea, E. J., Feingold, G., Ghan, S.,
413 Guenther, A. B., Kahn, R., Kraucunas, I., Kreidenweis, S. M., Molina, M. J., Nenes, A., Penner, J. E.,
414 Prather, K. A., Ramanathan, V., Ramaswamy, V., Rasch, P. J., Ravishankara, A. R., Rosenfeld, D.,
415 Stephens, G., and Wood, R.: Improving our fundamental understanding of the role of aerosol-cloud
416 interactions in the climate system, *Proc. Natl. Acad. Sci.*, 113, 5781–5790, doi:10.1073/pnas.1514043113,
417 2016.
418
- 419 Spracklen, D. V. and Rap, A.: Natural aerosol-climate feedbacks suppressed by anthropogenic aerosol,
420 *Geophys. Res. Lett.*, 40, 5316–5319, doi:10.1002/2013GL057966, 2013.
421
- 422 Stocker, T. F., Qin, D., Plattner, G. K., Tignor, M., Allen, S. K., Boschung, J., Nauels, A., Xia, Y., Bex, V., and
423 Midgley, P. M.: Summary for Policymakers, in: *Climate Change 2013: The Physical Science Basis*.
424 Contribution of Working Group I to the Fifth Assessment Report of the Intergovernmental Panel on
425 Climate Change, edited by Stocker, T. F., Qin, D., Plattner, G. K., Tignor, M., Allen, S. K., Boschung, J.,
426 Nauels, A., Xia, Y., Bex, V., and Midgley, P. M., Cambridge University Press, Cambridge, United Kingdom
427 and New York, NY, USA, 2013.
428
- 429 Tatzelt, C., Henning, S., Tummon, F., Hartmann, M., Baccharini, A., Welti, A., Lehtipalo, K. and Schmale, J.: Cloud
430 Condensation Nuclei number concentrations over the Southern Ocean during the austral summer of
431 2016/2017, Version 1.0 Data set, doi:10.5281/zenodo.2636765, 2019.
432
- 433 Tett, S. F. B., Rowlands, D. J., Mineter, M. J., and Cartis, C.: Can Top-Of-Atmosphere Radiation Measurements
434 Constrain Climate Predictions? Part II: Climate Sensitivity, *J. Climate.*, 26, 9367–9383, doi:10.1175/JCLI-
435 D-12-00596.1, 2013.
436
- 437 Wilcox, L. J., Highwood, E. J., Booth, B. B. B., and Carslaw, K. S.: Quantifying sources of inter-model diversity in
438 the cloud albedo effect, *Geophys. Res. Lett.*, 42, 1568–1575, doi:10.1002/2015GL063301, 2015.
439
- 440 Yoshioka, M., Regayre, L. A., Pringle, K. J., Johnson, J. S., Mann, G. W., Partridge, D., Stier, P., Kipling, Z.,
441 Bellouin, N., Sexton, D. M. H., Lister, G. M. S., Browse, J., Booth, B. B. B., Johnson, C. E., Johnson, B.,
442 Mollard, J. D. P., and Carslaw, K. S.: Ensembles of global climate model variants for the quantification and
443 constraint of uncertainty in aerosols and their radiative forcing, *J. Adv. Model. Earth Syst.*, Early Online
444 Release, doi:10.1029/2019MS001628, 2019.
445